RSC Advances

ROYAL SOCIETY OF CHEMISTRY

www.rsc.org/advances

TOC

In situ Synthesis of Graphene/Carbon Nanotube Modified Ordered Mesoporous Carbon as Protective Film of Stainless Steel Bipolar Plates for Proton Exchange Membrane Fuel Cells

Hairong Xue[a], Tao Wang[a, b, *], Hu Guo[a], Xiaoli Fan[a], Zetao Zhu[a], Xuchen Pan[a], Jianping He[a,*]

[a] College of Materials Science and Technology, Nanjing University of Aeronautics and Astronautics, 210016 Nanjing, PR China.

[b] World Premier International Research Center for Materials Nanoarchitectonics, National Institute for Materials Science, 1-1 Namiki, Tsukuba, Ibaraki 305-0044, Japan.

*Corresponding author. Tel: +86 25 52112900; Fax: +86 25 52112626.

E-mail address: WANG.Tao@nims.go.jp, jianph@nuaa.edu.cn

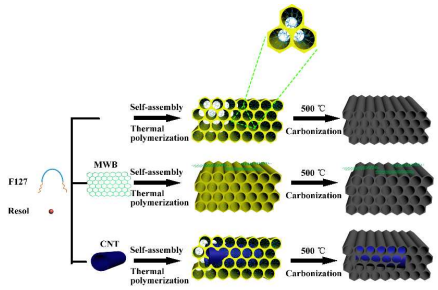

Graphene/CNT modified ordered mesoporous carbon films as protect coatings of the 304 stainless steel bipolar plate for PEFMCs by spin-coating.

RSC Advances

RSCPublishing

ARTICLE

In situ Synthesis of Graphene/Carbon Nanotube Modified Ordered Mesoporous Carbon as Protective Film of Stainless Steel Bipolar Plates for Proton Exchange Membrane Fuel Cells

Cite this: DOI: 10.1039/x0xx00000x

Received ooth January 2012,
Accepted ooth January 2012

DOI: 10.1039/x0xx00000x

www.rsc.org/

Hairong Xue[a], Tao Wang[a,b,*], Hu Guo[a], Xiaoli Fan[a], Zetao Zhu[a], Xuchen Pan[a], Jianping He[a,*]

Either graphene or carbon nanotube (CNT) is *in situ* introduced in ordered meseporous carbon film via spin-coating method, followed by evaporation-induced self-assembly of precursors and post calcinations. Graphene-modified and CNT-modified ordered mesoporous carbon films show improved electronic conductivity of 0.35 and 0.41 S m^{-1}, and contact angles of 90° and 96°, respectively, which are significantly higher than the values of 0.0043 S m^{-1} and 71° measured for the non-doped carbon film, suggesting enhanced graphitization degree and hydrophobic property. Two different hybrid carbon films deposited on 304 stainless steels as bipolar plates for proton exchange membrane fuel cells reveal remarkable corrosion resistance, which show very low corrosion current densities of 0.140 μA cm^{-2} and 0.008 μA cm^{-2}, respectively, in comparison with the 0.464 μA cm^{-2} measured on the bare 304 stainless steel. Such hybrid carbon films with preserved ordered mesporous structure and satisfactory electrochemical performance on 304 stainless steels can be considered as promising candidates for bipolar plate materials in proton exchange membrane fuel cells.

Introduction

Polymer electrolyte membrane fuel cells (PEMFCs) have been considered a promising environmentally-friendly technology for transportation and stationary applications，due to some attractive features such as high power density, quick startup, safety and low-temperature operation.[1-3] As a major critical component in PEMFCs, the bipolar plate not only provides structural support of the membrane electrode assembly, dissipates heat of the cells, and plays some pivotal roles of distributing and separating reactant gases, but also collects and transmits electric current. Therefore, high-quality bipolar plates can effectively increase output power density and lengthens service life of PEMFCs. With the purpose of being suited to use as bipolar plates, materials are required to have excellent electrical and thermal conductivity, high corrosion resistance, robust mechanical strength, negligible gas permeability, low manufacturing cost, and remarkable dimensional stability.[4-7] More studies showed that stainless steels, such as 304, 310, 316 and 321 stainless steels, may be promising metal bipolar plate materials for practical applications in PEMFCs, which possess high mechanical strength and low electrochemical resistance.[8, 9] However, stainless steel bipolar plates can easily form an oxide passivation layer on the surface of metal, contributing to increased surface contact resistance between bipolar plate and electrolyte. Whether this formed layer can protect the pure metal from further in-depth corrosion is still under debate. Moreover, in a weakly acidic and a high temperature operating environment, corrosion or dissolution of stainless steel can cause undesirable contamination of the entire membrane. Consequently, passivation and dissolution of stainless steel in operation will lead to reduced electronic conductivity and increased contact resistance, thus reduces the overall efficiency of PEMFCs.[10-12] A number of investigations reported that carbon-based coatings can effectively protect metal bipolar plates from corroding and prevent the augmentation of contact resistance in bipolar plates, thus maintaining the electrochemical performance of the fuel cell. Among various carbon materials, ordered mesoporous carbons may be promising coating candidates of metal bipolar plates due to high surface area and pore volume, uniform porous structure, and chemical inert surface.[13-15] However, because of the extensive existence of amorphous pore walls, mesoporous carbon materials usually possess lower graphitization degree and electronic conductivity than other commercial high graphitic carbon materials, such as carbon nanotubes and

graphene. Such imperfect structure has been a choke point and inhibits their industrial application as carbon-based coatings. Accordingly, making a breakthrough in PEMFCs is now an issue that needed to be addressed. Numerous research efforts have shown that electron-donating or electron-withdrawing elements doped in carbon skeleton, such as N, P and B, could change the electronic properties of carbon and produce additional functional groups on the carbon surface.[16-20] Though these modifications efficiently improve the thermal stability and other relevant properties of mesoporous carbon, the electrical conductivity and corrosion resistance remains low. Therefore, balancing these conflicting and inter-related requirements is still an intricate problem. In addition, fabricating a satisfactory ordered mesoporous carbon film with excellent abilities of excellent electron transport and corrosion inertness has not achieved yet.

According to unique characteristics of various carbon-based nanomaterials, graphene and carbon nanotube (CNT) can be selected as dopants to modify ordered mesoporous carbon. Graphene was first stripped from graphite by Novoselov *et al*. in 2004,[23] which shows a two-dimensional sheet composed of carbon atoms packed densely in a honeycomb crystal. CNT was discovered in the 1990s, which appears somewhat like a rolled-up graphene layer.[21, 22] Both of graphene and CNT have been utilized in numerous scientific fields due to their unique chemical and physical properties, [24] including high electrical conductivity,[21-22, 25] large surface area,[26] excellent mechanical strength,[27] and structural flexibility.[28] Owing to aforementioned advantages, they have extensively been demonstrated as useful doping elements or substrates to produce hybrid and composite materials in various applications, such as fuel cells,[29, 30] capacitors,[31, 32] catalysts,[33, 34] battery materials[35, 36] and solar cell,[37-39] and so on. There have been studies employing carbon nanotube and graphene to modify and optimize mesoporous carbon materials for improved electronic conductivity or other enhancements. In order to improve graphitization degree and conductivity of mesoporous carbon composites, Dai *et al.*[40] added some highly graphitized carbon materials such as carbon black, carbon onions, and carbon nanotubes during the synthesis of mesoporous carbon, in which resorcinol (or phloroglucinol) and formaldehyde were served as carbon precursors, and triblock copolymer F127 as soft template. These carbon composites as anode materials for lithium ion batteries showed better electrochemical performance than pure mesoporous carbon. Joo *et al.*[41] achieved ordered mesoporous carbon doped carbon nanotubes by using nickel phthalocyanine as carbon source and SBA-15 as hard template. The as-prepared nanocomposites possess a high surface area, which was attributed to the high porosity of ordered mesoporous carbon and three-dimensional crosslinked mesoporous structure. Moreover, carbon nanotubes could serve as a bridge for electron transportation within mesoporous carbon composites due to its high electric conductivity, resulting in excellent charge-discharge efficiency and stability in the applications of dye sensitized solar cell. Ozin *et al.*[42] synthesized periodic single-layer graphene oxide-mesoporous silica sandwich nanocomposites by doping graphene oxide into silicon oxide, which showed gas sensitive semi-conductive characteristics. In addition, our research group has demonstrated enhanced electrocatalytic performances by doping either graphene or CNT into ordered mesoporous carbon.[43, 44] The results indicated that moderate doping of graphene could optimize electrical conductivity of mesoporous carbon for improved catalytic performance.

To the best of our knowledge, there have been no reports on the practical use of graphitized carbon (graphene or carbon nanotube)-doped ordered mesoporous carbon composite films (MWG-OMC or CNT-OMC, respectively) as a protective coating on 304 stainless steels (304 SS). Herein, we report in situ synthesis of graphene/CNT modified mesoporous carbon hybrid films. Compared with physical vapour deposition (PVD), chemical vapor deposition (CVD) or electrolytic deposition methods, this in-situ synthesis has great advantages, such as convenience in use, low cost, large-area fabrication. Graphene (or carbon nanotube) can be successfully introduced into carbon precursors in the self-assembly stage of mesporous carbon. In situ synthetic approach contributes to not only uniform distribution of doping agent, but also well-reserved ordered mesoporous structure. As a protective coating of stainless steel bipolar plates, these modified carbon films were exposed to sulfuric acid solution to simulate acid environment of PEMFCs and their electrochemical behaviors have been evaluated by potentiodynamic and potentiostatic polarization methods. The improved performance has been achieved due to contributions from doping graphited carbon materials within ordered mesoporous carbon. Such modified carbon films have shown a promising application for the metallic plates in PEMFCs.

Experimental

Materials

Multi-walled carbon nanotubes (CNT) were purchased from Shenzhen Nanotech Port Co. Ltd (Shenzhen, China) with a diameter of 30~60 nm and length of 5~15 μm. Graphite powder, polystyrene sodium sulfonate (PSS) and triblock copolymer Pluronic F127 (M_w = 12600, $EO_{106}PO_{70}EO_{106}$) were purchased from Sigma-Aldrich Corp. Phenol, formalin solution (37 wt.%), H_2SO_4, NaOH, HCl, and ethanol were purchased from Shanghai Chemical Corp. All chemicals were analytical grade and used as received without any purification. Deionized water was used in all experiments. The compositions of the 304 SS are composed of C (0.08%), Mn (2.00%), P (0.045%), S (0.030%), Si (1.00%), Cr (18.0-20.0%), Ni (8.0-15.0%) and Fe (balance). The 304 SS is not low carbon stainless steel. The steel plates were cut into specimens of 5 * 5 cm, followed by grinding with 600-grit SiC paper and degreasing with acetone, then washing with distilled water and dried with warm air before the film coating process.

Synthesis of materials

Decoration of multi-walled carbon nanotubes (CNT)

Multi-walled carbon nanotube (CNT) exhibits poor dispersity in water and ethanol, and weak surface energy, so the CNT should be first modified to increase its surface energy and hydrophilicity. The original CNT was functionalized by stirring in 65 wt.% nitric acid at 110 ℃ for 48 h. The activated-CNT was obtained after rinsing with deionized water and drying in air at 100 ℃. Then, 0.1 g CNT was dispersed in 100 ml polystyrene sodium sulfonate (PSS) solution (10 wt.%). The solution was homogeneously mixed by stirring overnight, followed by successive ultrasonication for 3 h. We use PSS to form a negatively charged layer on the surface of CNT, which could stabilize the CNT in water through electrostatic repulsion. Finally, the PSS modified-CNT was collected via centrifugation, and washed with ethanol and deionized water for several times.[45]

Preparation of graphene

The synthesis of graphene is mainly composed of two steps: (1) graphene oxide (GO) was prepared from natural graphite by using a modified Hummers method. [46] In a typical preparation, 1 g graphite powder was put into 21 ml conc. sulfuric acid under stirring, and then 500 mg $NaNO_3$ was added into the suspension. The newly-formed mixture was powerfully stirred in an ice-bath at 0 ℃, followed by slowly adding 4 g $KMnO_4$. Simultaneously, the reaction temperature was kept below 20 ℃ by continuously stirring for 30 min. When the temperature was slowly elevated at 35 ℃, after stirring for additional 60 min, 46 ml water was added accompanying with increasing the temperature at 98 ℃. 140 ml water and 10 ml 30% H_2O_2 were further added to the above reaction solution after the other 15 min, and this final suspension was kept stirring at room temperature for 5 min more. The resulting products were collected after repeatedly centrifuging and washing with 5% HCl solution twice, followed by rinsing with distilled water. (2) Preparation of microwave expansion graphene (MWG) via microwave assisted reduction method. The as-prepared GO was irradiated by microwave for 3 min in the microwave oven (750 W) to strip the layers of the GO. Finally expanded and loose graphene powder was collected.

Preparation of graphene/CNT modified ordered mesoporous carbon films

The low-molecular-weight resol (phenol-form-aldehyde, M_w < 500) precursors were prepared according to the procedure reported by Zhao's group. [47] In a typical synthesis, 1.0 g Pluronic F127 was dissolved in 15.0 g anhydrous ethanol with vigorously stirring in 1 h at 40 ℃ to obtain a transparent solution. Meanwhile, 0.02 g MWG (or CNT) was well dispersed in 5.0 g anhydrous ethanol with ultrasonic treatments, , and then was transferred into the prepared F127/ethanol solution. After stirring in 10 min, the other 5.0 g resol (20% weight in ethanol) was dropwise added. The resulting black mixture was formed after stirring in 1h, and was coated on clean type 304 SS via spinning at 1500 rpm s^{-1} for 60 s. Such spin-coating was repeated for 5 times. The film-coated 304 SS was then subject to the evaporation of ethanol at room temperature overnight and thermopolymerization in an oven at 100 ℃ in 24 h in air. The heat treatment of 304 SS deposited with black film was carried out in a tubular furnace at 350 ℃ for 3 h, followed by at 500 ℃ for 2 h under N_2 atmosphere at a heating rate of 1 ℃ min^{-1}. Graphene/CNT modified mesoporous carbon film on 304 SS was obtained and denoted as MWG-OMC (or CNT-OMC).

Materials characterization

Structural and morphological characterization

The crystalline phases of the carbon films were identified through a Bruker D8 X-ray diffraction meter with monochromatic Cu K radiation (λ = 0.154056 nm) at 40 kV and 40 mA. Raman spectra were obtained by a french JY HR800 microscopic Raman system, using a He-Ne laser at an excitation wavelength of 633 nm. The porous structures of the carbon films were measured by an N_2 adsorption isotherm using a Micromeritics ASAP 2010 instrument at 77 K. The specific surface areas were calculated using the Brunauer-Emmet-Teller (BET) method. The Brunauer-Emmett-Teller (BET) method was utilized to calculate the specific surface areas based on adsorption data in the partial pressure (P/P_0) range 0.05-0.2. The pore volumes and pore size distributions derived from the desorption branches of isotherms were estimated based on Barett-Joyner-Halenda (BJH) model, the total pore volumes (V_{pore}) were computed from the adsorbed amount at a relative pressure (P/P_0) of 0.992. Water contact angles were measured by a contact angle system SL200B (SOLON. Tech., China). The Wentworth Laboratories 6514 System Electrometer Keithley was used to measure the in-plane electrical conductivity. The size and surface morphology of the carbon films were observed by using a Hitachi S-4800 field emission scanning electron microscopy (FESEM). Transmission electron microscopy (TEM) images were captured on the JEM-2100 instrument microscopy at an acceleration voltage of 200 kV to investigate the diameter and distribution of graphene or carbon nanotube within the ordered mesopores carbon framework as well as the characteristics of the order degree of mesopores carbon. The samples for TEM measurements were suspended in ethanol and supported on a holey carbon film on a Cu grid.

Electrochemical measurements

In electrochemical studies, a standard three-electrode cell was used with coated or uncoated 304 SS sheets as working electrode in a limited corrosion surface of 1 cm^2, a saturated Hg/Hg_2Cl_2 electrode (SCE) and a platinum foil as reference and counter electrodes. The electrodes were stabilized in the solution at open circuit for 60 min. An electrochemical interface (Solartron 1287) was employed to conduct potentiodynamic polarization, potentiostatic polarizations. Potentiodynamic polarizations were conducted at room temperature and at a scan rate of 10 mV s^{-1} in 0.5 mol L^{-1} H_2SO_4 aqueous solution or 0.5 mol L^{-1} H_2SO_4 aqueous solution bubbled with air (simulating the O_2 environmentin). The

potentiostatic polarizations were conducted at room temperature and recorded at potential of -100 mV (SCE) and +600 mV (SCE) in 0.5 mol L^{-1} H_2SO_4 aqueous solution. The applied potential of -100 mV (SCE) and +600 mV (SCE) are simulated the anode and the cathode of PEMFCs

Results and discussion

Structure characterization of OMC, WMG-OMC and CNT-OMC films

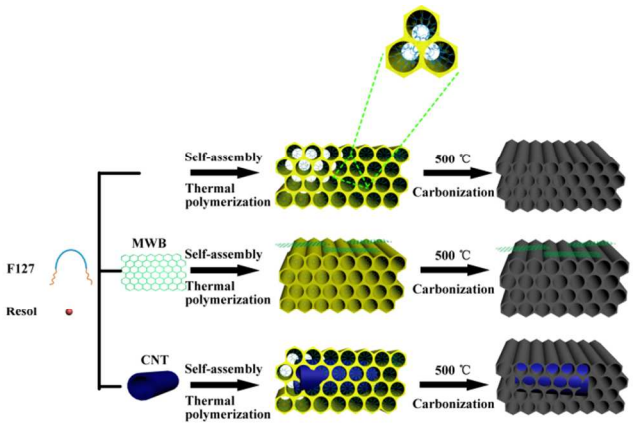

Fig. 1. Schematic diagram of preparation of ordered mesoporous carboned-films.

The formations of as-prepared OMC, and WMG or CNT modified OMC films are schematically illustrated in Fig 1. As we all know, spincoating-assisted evaporation-induced self-assembly (EISA) strategy is an appropriate method to fabricate uniform film.[13-15] The hybrid ordered mesoporous carbon films were synthesized by using F127 as the template, low-molecular-weight resol as the carbon source and treated MWG (or CNT) as the additives. During the self-assembly process of the resol precursor and triblock copolymer F127 micelles, either MWG or CNT can be combined with micelles via intermolecular forces or hydrogen bond through surface active groups including sulfo, hydroxyl, carboxyl and so on, thus forming regular spread on the surface of stainless steel substrates. Finally, the MWG-modified and CNT-modified ordered mesoporous carbon films were obtained by thermal polymerization and further pyrolysis of the F127 template as well as carbonization of the phenolic resin.

Fig. 2(a) shows the small-angle XRD patterns of the OMC, MWG-OMC and CNT-OMC, in which all patterns exhibit a well-defined diffraction peak attributed to (100) diffraction (at low-range 2θ ≈1°), indicating a long-range ordered two-dimensional hexagonal (p6mm) mesoporous structure. This result reveals that the presence of MWG (or CNT) has not obviously distorted the perfect ordered mesoporous structure. However, as compared with CNT-OMC, MWG-OMC shows the weaker diffraction peak in the low-angle region. Such phenomenon could be explained as follows: as a two-dimensional carbon material, although the MWG could be uniformly dispersed in ethanol, a certain amount of MWG may have an influence on the destabilizing consequences and inhomogeneous distribution of the triblock copolymer F127 micelles in the self-assembly process, due to its relative larger volume and surface area. The graphitization degree of different films is further investigated by wide-angle XRD pattern. As show in the built-in chart of Fig.2 (a), the wide-angle XRD patterns reveal broad diffraction peaks located around 18 ~ 23°, which are indexed to (002) diffraction attributed to the amorphous carbon. In addition, with MWG (or CNT) incorporated into the carbon framework, the diffraction peak of (002) shifts toward right closed to 2θ range of 26°, which indicates or implies the interatomic distance between carbon atoms of adjacent (002) is decreased. On the other hand, the pronounced peak at 43° can be indexed to the (101) reflections, pointing to the formation of graphite. This result indicates that MWG (or CNT), as a highly graphitized carbon material, deposited into the carbon framework can contribute to enhancing the graphitization degree of ordered mesoporous carbon film.

Fig. 2(b) shows Raman spectra of as-formed films. A distinct pair of vibrations at 1380 cm^{-1} (D band) and 1600 cm^{-1} (G band) can be observed of MWG-OMC and CNT-OMC. Raman spectroscopy is an effective characterization method to analyze the graphitization degree by distinguishing the ordered and disordered crystal structures of carbon. D band is a breathing mode of the k-point phonons of A_{1g} symmetry and related to the structure defects and disorders in the carbon materials, which is derived from the vibrations of sp^3-hybridized carbon atoms with dangling bonds in plane terminations of the disordered graphite. The G band is associated with the vibration of sp^2-bonded carbon atoms in the graphite layer, which reveals the carbon-carbon stretching (E_{2g}) mode of the hexagonal graphite. Therefore, the relative intensity ratio of I_D/I_G is proportional to the number of defect sites in graphite carbon, reflecting the graphitization degree of carbon films. The smaller I_D/I_G ratio shows the higher graphitization degree. As shown in Fig. 2(b), the signal of the Raman spectra for OMC is very weak, which indicates that the OMC is composed of incomplete carbonized phenolic resins due to the relatively low calcination temperature (500 ℃). For these hybrid carbon films, in comparison with OMC, both the D and G bands become sharper via incorporating either MWG or CNT in OMC structure, indicating a remarkable improvement for graphitization degree of the modified carbon films. This result is in agreement with wide-angle XRD characterizations (Fig. 2(a)). Because of relatively low additive amount, the signals of MWG-OMC and CNT-OMC are weaker than pure graphene and CNT (Fig. S1 of Supporting Information).The improved graphitization degree in modified OMC films can be ascribed to the high graphitization degree in MWG and CNT, resulting in improved holistic graphitization degree of the carbon films after doping them into the mesoporous carbon.

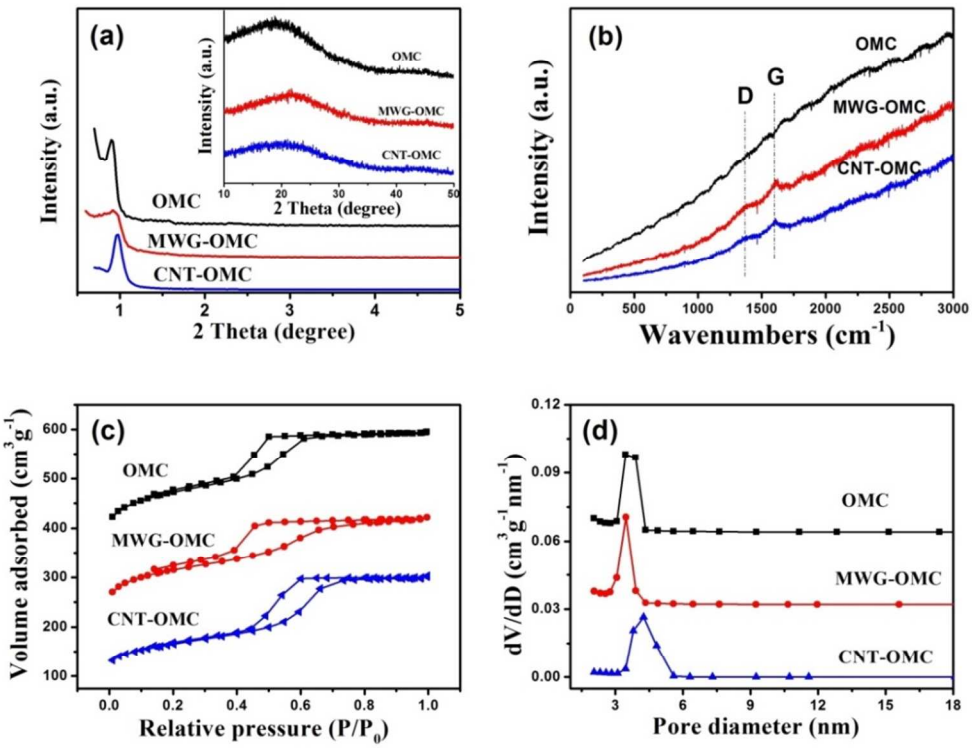

Fig. 2. Characterization of OMC, WMG-OMC and CNT-OMC films: (a) Small-angle XRD and Wide-angle XRD (the built-in chart) patterns; (b) Raman spectra; (c) N_2 adsorption-desorption isotherm; (d) corresponding pore size distributions calculated by BJH method from both branches.

Further details regarding porosities of the intriguing hybrid carbon films were obtained through nitrogen adsorption measurements. As shown in Fig. 2(c), the N_2 adsorption-desorption curves obtained from these films exhibit typical IV shapes with H1-type hysteresis loops.[47, 48] The noteworthy nitrogen uptake at the relative pressure P/P_o range of 0.40 ~ 0.70 is the typical capillary condensation of nitrogen in the mesoporous materials with one-dimensional cylindrical channels. By using the Barrett-Joyner-Halenda (BJH) model, desorption pore-size distribution curves of the films calculated from the desorption branch are shown in Fig. 2(d). Narrow pore-size distributions of OMC, MWG-OMC and CNT-OMC center at about 3.1 nm, 3.0 nm and 3.5 nm, respectively, indicating that all the films have very uniform mesoporous structure. Table 1 summarizes the pore sizes (D), BET surface areas (S_{BET}) and total pore volumes (V_{total}) of films calculated from the N_2 adsorption-desorption data are. The textural parameters of MWG-OMC and CNT-OMC are very similar to OMC, implying that ordered mesoporous structure of the films can be reserved when moderate MWG (or CNT) are embedded in it. However, the specific surface area and pore size of MWG (559 $m^2 g^{-1}$, 3.0 nm) decreases as compared with OMC (588 $m^2 g^{-1}$, 3.1 nm), which might be caused by wrapping or covering a part of ordered mesoporous channels with graphene sheets. In addition, the increased microporous clearances decrease the total pore volume (0.42 $cm^3 g^{-1}$) and the proportion of mesoporous (70.9%). Differently, the ordered mesoporous carbon film modified with CNT has an increased pore size (3.4 nm). As we known, CNT possesses one-dimension linear structure, which may disperse into mesoporous carbon skeleton and enlarged the channels in partial region, and thus leading graphene to widen the pore size distribution. These N_2 adsorption-desorption data are consistent with the previous discussion of Low-angle XRD (Fig. 2(a)) and subsequent analysis of TEM (Fig. 3) results.

Table. 1. The structural parameters of OMC, WMG-OMC and CNT-OMC films

Sample	S_{BET} ($m^2 g^{-1}$)	V_{total} ($cm^3 g^{-1}$)	R_{meso} (%)	D (nm)
OMC	588	0.46	76.1%	3.1
MWG-OMC	559	0.42	70.9%	3.0
CNT-OMC	553	0.47	79.2%	3.4

The structural characterization was further carried out with the TEM and HRTEM measurements for the OMC, WMG-OMC and CNT-OMC films. It can be clearly seen in Fig. 3(a) that, in the (001) direction, the order honeycomb-like pore structure of OMC corresponds to a two-dimension hexagonal (p6mm) structure. In addition, in the corner of the OMC, the highly ordered parallel mesoporous channels can be observed by viewing along (110) direction, which is consistent with the results of low-angle XRD (Fig. 2(a)). The TEM images of CNT-OMC are shown in Fig. 3 (b) and (c) show. The ordered one-dimensional nano-channels of ordered mesoporous carbon are remained, while the order degree of the pore structure is

reduced. A small number of CNT (yellow circle) obtained by acid oxidation assisted with PSS modification, dispersed on the surface or inside of the mesopores carbon skeleton are also observed. As shown in Fig. 3 (d, e), the thin strip-shaped MWG sheets (yellow box) spread over the ordered mesoporous carbon film, and a few MWG sheets dispersed through the carbon skeleton can also be captured. The HRTEM image (Fig. 3(f)), magnified image of Fig. 3(e) (yellow box), shows a regular fingerprint, which is the typical characteristic of the graphitized structure of graphene. The unit cell parameter of MWG sheets estimated from the HRTEM is about 3.4 nm. This result indicates that the MWG-OMC (or CNT-OMC) has been successfully prepared by modifying with the MWG (or CNT), so the carbon films will possess a higher graphitization degree and better conductivity than OMC due to the excellent conductivity of highly graphitized MWG (or CNT). In addition, the conductivity of the films obtained from four point probe technique is shown in Table 2. Obviously, after modifying with MWG (or CNT), the electrical conductivity of the carbon films can be efficiently improved.

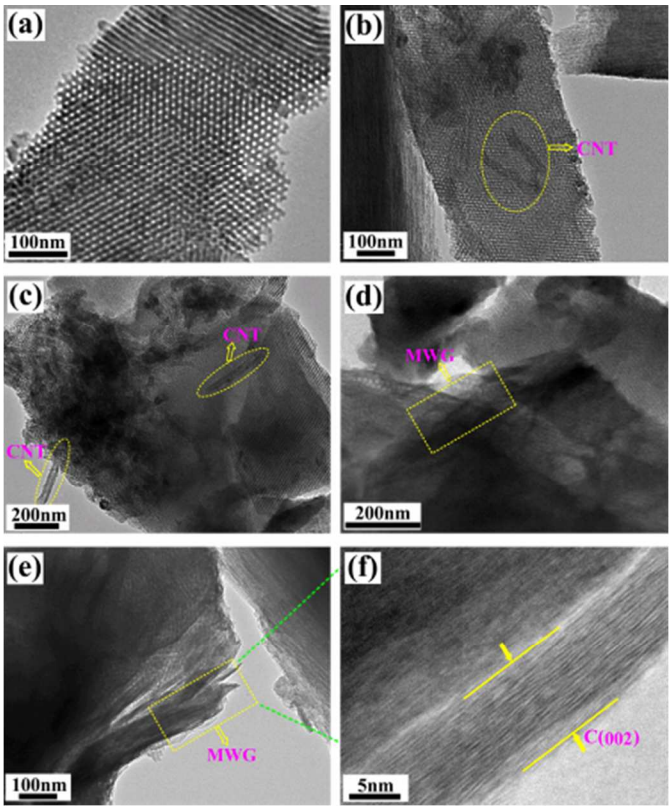

Fig. 3. TEM images of OMC, WMG-OMC and CNT-OMC films: (a) OMC, (b,c) CNT-OMC, (d,e,f) MWG-OMC.

A more detailed structural characterization was revealed by FE-SEM measurement. As shown in Fig. 4(a), it can be observed that the OMC exhibits large-domain regular ordered two-dimensional mesoporous channels. Moreover, the surface of OMC film is very smooth. The image (Fig. 4(b)) of MWG-OMC shows that the MWG modified film remains ordered mesoporous framework, whereas the surface of MWG-OMC becomes rough and the thin strip-shaped MWG sheets can be seen around the mesoporous channels. However, owing to the smaller size of CNT compared with MWG, we do not observe obvious CNT in the channel structure from Fig. 4(c). However, some changes of the mesoporous carbon skeleton can be still found, including rough surface and enlarged channels occurred in some areas of the film. These results indicate that the ordered mesoporous structure cannot be drastically distorted by doping MWG (or CNT). Moreover, enhanced roughness after introduction of carbon additives into OMC films is favorable for improved hydrophobicity of hybrid films.

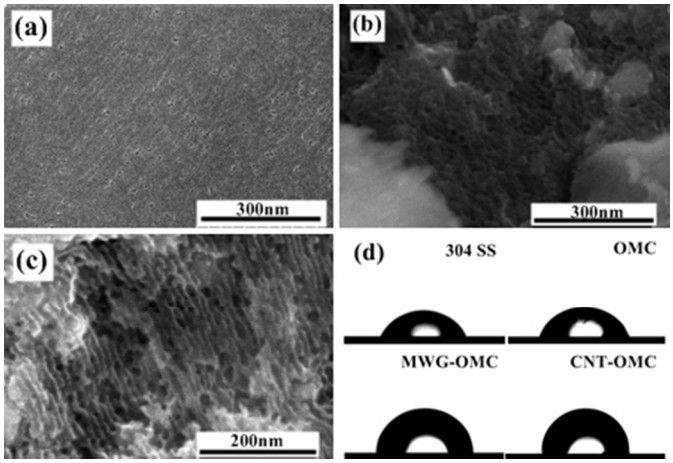

Fig. 4. SEM images of OMC, WMG-OMC and CNT-OMC films: (a) OMC, (b) MWG-OMC, (c) CNT-OMC; (d) The water contact angle of OMC, WMG-OMC and CNT-OMC films.

Surface property and electrical conductivity of bipolar plates have a prominent effect on PEMFCs performances at high current densities. The water is produced by the cathode oxygen reduction reaction in operation, which should be removed in time in order to prevent blocking the reactant gases access to the electrode and submerging the catalyst. These carbon films are applied to protect the surface of stainless steel bipolar plates for PEMFCs, so low surface energy, high water contact angle (>90°) and low surface wetability of the carbon films are obviously beneficial to remove water derived from the cathode side of the fuel cell.[13-14, 49] Some previous researches have reported that hydrophilic groups of the carbon films can transfer to volatile small-molecules by carbonizing. After increasing the graphitization degree of the carbon films during synthesis process, the surface of the carbon films will consist of nonpolar graphitic carbon and then possess better hydrophobicity. Therefore, the same as electrical conductivity, the surface property of carbon films is conducted to demonstrate the graphitization degree of the carbon films. The surface property and electrical conductivity are collected in Table 2, and the water contact angles of the carbon films are shown in Fig. 4(d). The contact angle increases with improvement of the hydrophobicity. Generally, the contact angle value of the uncoated 304 SS is approximately 60~70° due to some hydrophilic groups existed on the surface. As show in Fig. 4(d) and Table 2, the 304 SS coated with an OMC film

by spinning method has a contact angle of 71°. Compared to uncoated 304 SS, whose contact angle value is 64°, this slight increase may be attributed to the reduced hydrophilicity. On the basis of our previous studies, graphitized modification of carbon film can increase the contact angle to 80° ~ 90° by doping with B, N, P, Mo and so on.[15,50-53] In this research, adding MWG into OMC film followed by high-temperature heat treatments can improve whole graphitization degree of hybrid carbon film. Simultaneously, the decrease of active functional groups and the formation of rough microstructure on the surface of the MWG-OMC can also reduce the hydrophobicity. Therefore, the water contact angle of MWG-OMC can be increased to 90°, and the electrical conductivity is much higher than OMC (Table 2). In addition, as shown in Table 2, CNT-OMC owns the highest water contact angle and electrical conductivity, suggesting that CNT can remarkably promote the graphitization degree of carbon film, in consistent with the results of wide-angle XRD patterns and Raman spectra. Besides, this rough micro/nanostructure of the films could greatly improve the surface hydrophobic property (water contact angle at 96°). Above all, the MWG/CNT modified ordered mesoporous carbon film has larger water contact angle than pure ordered mesoporous carbon film, contributing to enhanced protective performance of these hydrophobic carbon films in acidic aqueous solution for PEMFCs. Moreover, electrical conductivity of bipolar plates has a prominent effect on PEMFCs performances at high current densities. Compare to the electrical conductivity of ordered mesoporous carbon film (0.0043 S m^{-1}), the conductivity of MWG/CNT modified ordered mesoporous carbon film is increased to 0.35 or 0.41 S m^{-1} due to the higher conductivity of MWG or CNT.

Table. 2. The values of contact angles with water and electrical conductivity of OMC, WMG-OMC and CNT-OMC films.

Sample	Contact angle (°)	Surface energy (N m^{-2})	G (S m^{-1})
304 SS	61	40.4	-
OMC	71	32.0	0.0043
MWG-OMC	90	18.5	0.35
CNT-OMC	96	14.8	0.41

Electrochemical polarization measurements of OMC, WMG-OMC and CNT-OMC films

These protective films are applied to coat on the surface of the 304 SS as a protective layer. In order to analyze the electrochemical behavior in the simulated working environment of PEMFCs, the films coated 304 SS was immersed in 0.5 mol L^{-1} H_2SO_4 aqueous solution for 1 h. When the surface state of working electrode was basically stable, we could evaluate the protective performance of the films by potentiodynamic polarization curves, as shown in Fig. 5. The corrosion current (i_{corr}) and corrosion potential (E_{corr}) calculated by potentiodynamic polarization extrapolations for these films are summarized in Table 3. E_{corr} and i_{corr} of the OMC coated 304 SS are 91 mV (SCE) and 0.464 μA cm^{-2}, respectively, exhibiting well protective perfomance in 0.5 mol L^{-1} H_2SO_4 solution. The increased E_{corr} is found from the MWG-OMC-coated 304 SS which shows a shift to a more positive value by about 247 mV (SCE), and the i_{corr} is measured of 0.140 μA cm^{-2}, much lower than 0.464 μA cm^{-2} of OMC. Moreover, CNT-OMC-coated 304 SS displays maximized protective performance, including the most positive E_{corr} of 406 mV (SCE) and lowest i_{corr} of 0.008 μA cm^{-2}. Our recent work shows significant enhanced protective performance in comparison with previous achievements.[14, 15] For example, we have reported that an ordered mesoporous boron-containing carbon film coated on 304 SS shows well protective performance, corresponding E_{corr} and i_{corr} are 183 mV and 0.285 μA cm^{-2}, respectively.[15] We also successfully prepared mesoporous C-SiO_2-N films coated on 304 SS, whose E_{corr} and i_{corr} are 292 mV and 0.13 μA cm^{-2}, respectively.[14] The test data indicates that the corrosion resistance of 304 SS significantly increases with OMC layer in 0.5 mol L^{-1} H_2SO_4 solution, even which can be further enhanced by modifying with MWG (or CNT). The improved electrochemical performance can be probably ascribed to the introduction of the high graphitized CNT (or MWG) in appropriate contents, which not only can be well dispersed in ordered mesoporous structure but also enhance the stability due to its perfect compact structure. Furthermore, deposition of MWG (or CNT) within OMC films can increase the hydrophobicity of composite carbon films. The improved graphitization degree can effectively enhance the electric conductivity, and the excellent hydrophobic properties can increase the contact angles with water. As a result, the hybrid carbon films exhibit well protective performance. As we all know, the bipolar plates are usually used in H_2 or O_2 atmophere in PEMFC. So, we also investigate the protective performance of the films in 0.5 mol·L^{-1} H_2SO_4 aqueous solution bubbled with air (simulating the O_2 environmentin). As shown in Fig. S2 and Table S2, the protective performance of the carbon films in 0.5 mol·L^{-1} H_2SO_4 aqueous solution bubbled with air is similar to that in 0.5 mol L^{-1} H_2SO_4 aqueous solution, although the corrosion current densities of films show slightly increase and the corrosion potentials show a shift to a more negative value a little.

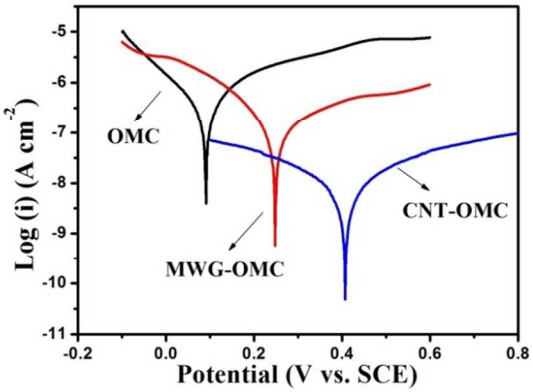

Fig. 5. Potentiodynamic polarization curves of OMC, WMG-OMC and CNT-OMC films in 0.5 mol L^{-1} H_2SO_4 solution.

Potentiostatic polarization measurement was used to preliminary evaluate the stability performance of the OMC, WMG-OMC and CNT-OMC films. As aforementioned, in actual working conditions of PEMFC, the anode potential is at -100 mV (SCE) and while the cathode potential is at +600 mV (SCE). Therefore, the bipolar plates undergo corrosion at an applied potential which is different from the free potential corrosion. Fig. 6 (a) shows the potentiostatic polarization curves of the as-prepared films-coated 304 SS in 0.5 mol L^{-1} H_2SO_4 solution at +600 mv (SCE). The polarization current density of OMC decreased slowly with time to the level of 1.3 μA cm^{-2} in 1 h, while the polarization currents of MWG-OMC and CNT-OMC decreased immediately with time to the level of 0.08 μA cm^{-2} and 0.009 μA cm^{-2} respectively, obviously lower than the passive current for the OMC. Furthermore, the films modified with MWG (or CNT) exhibits favorable stability during the polarization, which can be evidenced by that the absence of the current density fluctuation and no degradation of current density is observed after potentiostatic measurements. The results indicate that the modified mesoporous carbon films are very stable at the cathode working potential for PEMFC. Fig. 6 (b) is the potentiostatic polarization curves for the ordered mesoporous carbon films coated 304 SS in 0.5 mol L^{-1} solution at -100 mv (SCE). Obviously, the polarization current densities of the films all decrease immediately with time to a steady value of -2.8、-0.98 and -0.26 μA cm^{-2} for OMC, MWG-OMC and CNT-OMC, respectively. The negative current density is attributed to the reduction of H^+ ions that changes to H_2 and provides cathodic protection for the coated 304 SS. No degradation is observed after potentiostatic measurements for 1 h, indicating the high stability of the films at the anode working potential of PEMFCs, especially MWG-OMC and CNT-OMC. These modified ordered mesoporous carbon films effectively protect the substrate steel from corrosion. In addition, the mesoporous films were further tested for about 6 hours at 600 mV (SCE) in 0.5 mol L^{-1} H_2SO_4 solution to judge the stability of the films. As shown from Fig. S3, the trends indicate that the mesoporous films would be stable even after 6 hours.

Table. 3. The corrosion current density (I_{corr}) and the corrosion potentials (E_{corr}) values for OMC, WMG-OMC and CNT-OMC films. in 0.5 mol L^{-1} H_2SO_4

Sample	E_{corr} (mV)(SCE)	i_{corr} (μA cm^{-2})
OMC	91	0.464
MWG-OMC	247	0.140
CNT-OMC	406	0.008

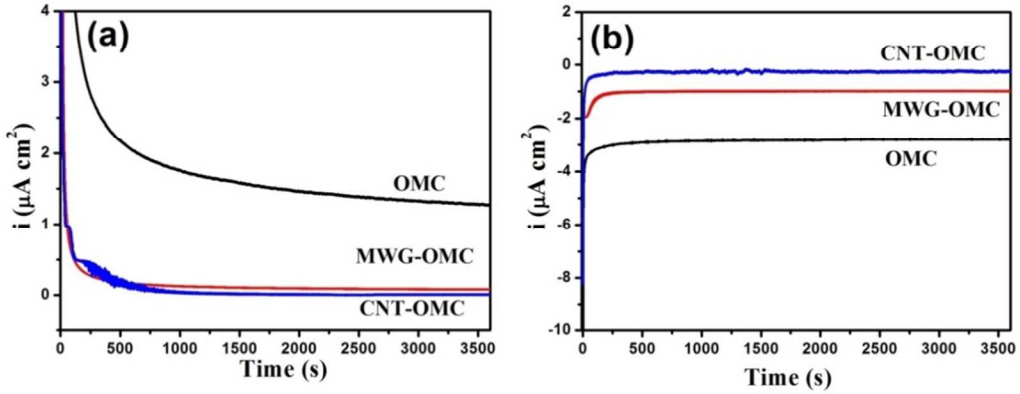

Fig. 6. Potentiostatic polarization curves of OMC, WMG-OMC and CNT-OMC films at (a) 600 mV (SCE), (b) -100 mV (SCE) in 0.5 mol L^{-1} H_2SO_4solution.

Conclusions

MWG and or CNT have been successfully introduced into ordered mesoporous carbon by an in situ process. The obtained materials (MWG-OMC and CNT-OMC) preserve an ordered two-dimensional mesoporous structure with corresponding high surface area. The modified ordered mesoporous carbon composite shows a higher graphitization degree both in MWG-OMC and CNT-OMC in comparison with the pristine OMC. As protective coatings of bipolar plate materials, 304 SS coated with these prepared carbon hybrid films have excellent protective performance in 0.5 M H_2SO_4 corrosion system to simulate acid environment of PEMFCs as compared with OMC film. The introduction of MWG or CNT can noticeably improve the graphitization degree of carbon films. Moreover, the rough micro/nanocomposite structures formed from the modifications of MWG or CNT result in hydrophobicity of coating surface, and the high surface tension with water contact angle is close to 90°. Consequently, the electrochemical performance of carbon film can be obviously improved. MWG-OMC and CNT-OMC films show the enhanced protection performance. The corresponding corrosion potentials of MWG-OMC and CNT-OMC can be measured of 247 mV (SCE) and 406 mV (SCE), respectively. Moreover, MWG-OMC and CNT-OMC show low corrosion current densities of 0.140 μA cm^{-2} and 0.008 μA cm^{-2}, respectively. The electric conductivity for both modified carbon films can be as high as 0.35, and 0.41 S m^{-1}, respectively. The excellent performance indicates that these graphene-modified and CNT-modified ordered mesoporous carbon conductive composite films have a potential application as a protective coating of bipolar plate materials.

Acknowledgements

The authors appreciate the financial support from the National Natural Science Foundation of China (51372115).

Notes and references

[a] *College of Materials Science and Technology, Nanjing University of Aeronautics and Astronautics, 210016 Nanjing, PR China.*
b World Premier International Research Center for Materials Nanoarchitectonics, National Institute for Materials Science, 1-1 Namiki, Tsukuba, Ibaraki 305-0044, Japan.
Tel: +86 25 52112900; Fax: +86 25 52112626.
E-mail address: jianph@nuaa.edu.cn

1 V. Mehta and J.S. Cooper, *J. Power Sources*, 2003, **1**, 32-53.
2 A. Schafer, J.B. Heywood and M.A. Weiss, *Energy*, 2006, **31**, 2064-2087
3 C. Galeano, J.C. Meier, V. Peinecke, H. Bongard, I. Katsounaros, A.A. Topalov, A. Lu, K.J.J. Mayrhofer and F. Schüth, *J. Am. Chem. Soc.*, 2012, **134**, 20457-20465.
4 T.M. Wena, K.H. Hou, C.Y. Bai, M.D. Ger, P.H. Chien and S.J. Lee, *Corros. Sci.*, 2010, **52**, 3599-3608.
5 R.F. Silva, D. Franchi, A. Leone, L. Pilloni, A. Masci and A. Pozio, *Electrochim. Acta*, 2006, **51**, 3592-3598.
6 Y.J. Ren and C.L. Zeng, *J. Power Sources*, 2008, **182**, 524-530.
7 Y.J. Ren, J. Chen and C.L. Zeng, *J. Power Sources*, 2010, **195**, 1914-1919.
8 A. Schafer, J.B. Heywood and M.A. Weiss, *Energy,* 2006, **31**, 2064-2087.
9 R.F. Silva, D. Franchi, A. Leone, L. Pilloni, A. Masci and A. Pozio, *Electrochim. Acta*, 2006, **51**, 3592-3598.
10 J. Wind, R. Späh, W. Kaiser and G. Böhm, *J. Power Sources*, 2002 **105**, 256-260.
11 H. Tawfik, Y. Hung and D. Mahajan, *J. Power Sources*, 2007, **163**, 755-767.
12 R.A. Antunes, M.C.L. Oliveira, G. Ett and V. Ett, *Int. J. Hydrogen Energy*, 2010, **35**, 3632-3647.
13 T. Wang, J.P. He, D. Sun, J.H. Zhou, Y.X. Guo, X.C. Ding, S.C. Wu, J.Q. Zhao and J. Tang, *Corros. Sci.*, 2011, **53**, 1498-1504.
14 T. Wang, J.P. He, D. Sun, Y.X. Guo, Y.O. Ma, G.X. L, H.R. Xue, J. Tang and X. Sun, *J. Power Sources*, 2011, **196**, 9552-9560.
15 T. Wang, C.X. Zhang, X. Sun, Y.X. Guo, H. Guo, J. Tang, H.R. Xue, M.Z. Liu, X.X. Zhang, L. Zhu, Q.Q. Xie and J.P. He, *J. Power Sources*, 2012, **212**, 1-12.
16 R.L. Liu, D.Q. Wu, X.L. Feng and K. Müllen, *Angew. Chem. Int. Ed.*, 2010, **49**, 2565-2569.
17 D. Hulicova-Jurcakova, M. Kodama, S. Shiraishi, H. Hatori, Z.H. Zhu and G.Q. Lu, *Adv. Funct. Mater.*, 2009, **19**, 1800-1809.
18 J. Zhang, X. Liu, R. Blume, A. Zhang, R. Schlogl and D.S. Su, *Science*, 2008, **322**, 73-77.
19 Y. Li, J. Zhong, X.Z. Yang, G.J. Lan, H.D. Tang and H.Z. Liu, *New Carbon Mater.*, 2011, **26**, 123-129.
20 B.F. Abramovic, L.J. Bjelica, F.F. Gaal, V.J. Guzsvany and L.S. Jovanovic, *Electroanalysis*, 2003, **15**, 878-884.
21 C.D. Liang and S. Dai, *J. Am. Chem. Soc.*, 2006, **128**, 5316-5317.
22 A. Izadi-Najafabadi, T. Yamada, D.N. Futaba, D.N. Futaba, M. Yudasaka, H. Takagi, H. Hatori, S. Lijima and K. Hata, *ACS Nano*, 2011, **5**, 811-819.
23 K.S. Novoselov, A.K. Geim, S.V. Morozov, D. Jiang, Y. Zhang, S. V. Dubonos, I. V. Grigorieva and A. A. Firsov, *Science*., 2004, **306**, 666-669.
24 S. Bose, T. Kuila, A. K. Mishra, R. Rajasekar, N. H. Kim and J. H. Lee, *J. Mater. Chem*., 2012, **22**, 9696-9703.
25 X. Du, I. Skachko, A. Barker and E. Y. Andrei, *Nat. Nanotechnol.*, 2008, **3**, 491-495.
26 S. Stankovich, D. A. Dikin, G. H. B. Dommett, K. M. Kohlhaas, E. J. Zimney, E. A. Stach, R. D. Piner, S. T. Nguyen and R. S. Ruoff, *Nature*, 2006, **442**, 282-286.
27 C. Lee, X. Wei, J. W. Kysar and J. Hone, *Science*, 2008, **321**, 385-388.
28 A. K. Geim, *Science*, 2009, **324**, 1530-1534.
29 Y. C. Si and E. T. Samulski, *Chem. Mater.*, 2008, **20**, 6792-6797.
30 B. Seger and P. V. Kamat, *J. Phys. Chem. C*, 2009, **113**, 7990-7995.
31 H. Gao and K. Lian, *RSC Adv.*, 2014, **4**, 33091-33113.
32 Y.Z Fang, F.T. Jiang, H. Liu, X.M. Wu and Y. Lu, *RSC Adv*., 2012, **2**, 6562-6569.
33 R.K. Upadhyay, N. Soin and S. S. Roy, *RSC Adv.*, 2014, **4**, 3823-3851.
34 G.X. Zhao, T. Wen, C.L. Chen and X.K. Wang, *RSC Adv.*, 2012, **2**, 9286-9303.
35 T. Tao, M. M. Rahman, T. Ramireddy, J. Sunarso, Y. Chen and A. M. Glushenkov, *RSC Adv.*, 2014, **4**, 36649-36655.
36 T.Q. Chen, L.K. Pan, X.J. Liu, K. Yu and Z. Sun, *RSC Adv.*, 2012, **2**, 11719-11724.
37 C.P. Liu, Y.Y. Hui, Z.H. Chen, J.G. Ren, Y. Zhou, L.B. Tang, Y.B. Tang, J. A. Zapien and S.P. Lau, *RSC Adv.*, 2013, **3**, 17918-17923.
38 G. D. Sharma, D. Daphnomili, K. S. V. Gupta, T. Gayathri, S. P. Singh, P. A. Angaridis, T. N. Kitsopoulos, D. Tasis and A. G. Coutsolelos, *RSC Adv.*, 2013, **3**, 22412-22420.
39 K.F. Wang, S.J. Wan, Q.Q. Liu, N.L. Yang and J. Zhai, *RSC Adv.*, 2013, **3**, 23755-23761.
40 B.K. Guo, X.Q. Wang, P.F. Fulvio, M.F Chi, S.M. Mahurin, X.G. Sun and S. Dai, *Adv. Mater.*, 2011, **23**, 4661-4666.
41 P.F. Fulvio, R.T. Mayes, X.Q. Wang, S.M. Mahurin, J.C. Bauer, V. Presser, J. McDonough, Y. Gogotsi and S. Dai, *Adv. Funct. Mater.*, 2011, **21**, 2208-2215.
42 Y. Jo, J.Y. Cheon, J. Yu, H.Y. Jeong, C.H. Han, Y.S. Jun and S.H. Joo, *Chem. Commun.*, 2012, **48**, 8057-8059.
43 Z.M. Wang, W.D. Wang, N. Coombs, N. Soheilnia and G.A. Ozin, *ACS Nano*, 2010, **4**, 7437-7450.
44 X. Sun, J.P. He, J. Tang, T. Wang, Y.X. Guo, H.R. Xue, G.X. Li and Y.O. Ma, *J. Mater. Chem.*, 2012, **22**, 10900-10910.
45 X.X. Zhang, J.P. He, T. Wang, M.Z. Liu, H.R. Xue, H. Guo, *J. Mater. Chem. A*, 2014, **2**, 3072-3082.
46 R.K. Sharma and L. Zhai, *Electrochim. Acta*, 2009, 54, 7148-7155.
47 W.S. Hummers and R.E. Offeman, *J. Am. Chem. Soc.*, 1958, **80**, 1339-1339.
48 D.Y. Zhao, J.L. Feng, Q.S. Huo, N. Melosh, G.H. Fredrisckson, B.F. Chmelka and G.D. Stucky, *Science*, 1998, **279**, 548-552.
49 D.Y. Zhao, J.Sun, Q. Li and G.D. Stucky, *Chem. Mater.*, 2000, **12**, 275-279.

50 H. Tawfik, Y. Hung and D. Mahajan, *J. Power Sources*, 2007, **163**, 755-767.
51 M.Z. Liu, T. Wang, X.X. Zhang, X.L. Fana, J. Tang, Q.Q Xie, H.R Xue, H. Guo and J.P. He, *Corros. Sci*. 2014. **87**. 297-305.
52 T. Wang, J. Tang, X.L. Fan, J.H. Zhou, H.R. Xue, H. Guo and J.P. He, *Nanoscale*, 2014, **6**, 5359-5371.
53 J. Tang, T. Wang, X.C. Pan, X. Sun, X.L. Fan, Y.X. Guo, H.R. Guo and J.P. He, *J. Phys. Chem. C*, 2013, **33**, 16986-16906.
54 J. Tang, T. Wang, X. Sun, Y.X. Guo, H.R. Xue, H. Guo, M.Z. Liu, X.X. Zhang and J.P. He, *Micropor. Mesopor. Mater.*, 2013, **177**, 105-112

